DESIGN OF ADVANCED BAINITIC STEELS BY OPTIMISATION OF TTT DIAGRAMS AND T_O CURVES

Francisca G. Caballero, María Jesús Santofimia, Carlos Capdevila, Carlos García-Mateo and Carlos García de Andrés.

Materalia Research Group, Department of Physical Metallurgy, Centro Nacional de Investigaciones Metalúrgicas (CENIM), Consejo Superior de Investigaciones Científicas (CSIC), Avda. Gregorio del Amo, 8. E-28040 Madrid, Spain

Synopsis

Cementite is responsible of the limited application of conventional bainitic steels, however it has been proof that cementite precipitation during bainite formation can be suppressed by the judicious use of silicon in medium carbon steels. In this work, thermodynamic and kinetic models were used to design steels with an optimum bainitic microstructure consisting of a mixture of bainitic ferrite, carbon-enriched retained austenite and some martensite. Using these models, a set of seven carbide free bainitic steels with a 0.3 wt-% carbon content were proposed for manufacturing. The work presented here is concerned with the microstructural and mechanical characterisation of the steels manufactured. Except for the steel with the highest content of alloying elements, all the grades present the same microstructure composed of carbide-free upper bainite and retained austenite after hot rolling and a two-steps cooling. Theirs tensile strengths range from 1600 MPa to 1950 MPa while keeping a uniform elongation equal to 4 % and a total elongation over 10 %. Regarding toughness at room temperature, they match quenched and tempered martensitic steels.

Keywords

Steels; Bainite; Materials Design; TTT curve; Incomplete reaction; Modelling.

1. Introduction

Conventional bainitic steels exhibited quite reasonable combinations of toughness and strength, but compare unfavourably with quenched and tempered martensitic steels. The presence of cementite has a detrimental effect in the microstructure since cementite particles are responsible for damage initiation in high-strength steels. However, the precipitation of cementite during bainitic transformation can be suppressed by alloying the steel with about 2 wt-% of silicon, which has very low solubility in cementite and greatly retards growth of cementite from austenite. The carbon that is rejected from the bainitic ferrite enriches the residual austenite, thereby stabilising it down to room temperature. The resulting microstructure consists of fine plates of bainitic ferrite separated by carbon-enriched regions of austenite. There may also be some martensite present.

The advantages of obtaining this type of microstructure in flat products are manifold. Because of the ultra fine grain size of the bainitic ferrite plates, there is a possibility of improving simultaneously the strength and toughness, while keeping sufficient ductility for forming and showing a high resistance to damage. The high flow stresses are due to the absence of proeutectoid ferrite contrary to existing TRIP (transformation induced plasticity) steels and to the low thickness of the bainitic laths. The TRIP effect expected from the residual austenite and the presence of islands of martensite lead to high instantaneous hardening rates. The in-use properties, such as toughness, resistance to damage, fatigue and sensibility to cut-edge are also noteworthy. The achieved combinations of properties are of great interest for the design of safety parts in automotive industries.

In spite of all these potential advantages, the carbide-free bainitic microstructure has on some occasions failed to live up to its expectations. This is primarily because of the instability of relatively large or blocky regions of austenite, which become trapped between sheaves of bainite. Therefore, every effort has to be made to reduce the fraction of blocky austenite and increase its stability to martensitic transformation. The aim of alloy design should then be to increase the maximum permitted amount of transformation to bainitic ferrite. There may be other constraints, for example, the need to ensure that the hardenability of the steel is sufficient for avoiding proeutectoid ferrite formation during cooling. In this sense, thermodynamic and kinetic models were used to design steels with an optimum bainitic microstructure for avoiding large regions of austenite and proeutectoid ferrite. These models also helped to select an optimum processing route for these steels.

Previous research, carried out by Bhadeshia and Edmonds[1,2] and Miihkinen and Edmonds[3-5], on two silicon-containing steels, nominally, Fe-0.2C-2Si-3Mn wt-% and Fe-0.4C-2Si-4Ni wt-%, showed that these alloys are promising. The Fe-0.2C-2Si-3Mn wt-% alloy exhibited excellent fracture toughness (K_{Ic}=125 MPa$\sqrt{m}$) in a yield strength range of 1000-1100 MPa as isothermally heat-treated between 350ºC and 300^{o}C. Because of the increased carbon content, higher strength levels (1200-1400 MPa) were obtained in the Fe-0.4C-2Si-4Ni wt-% alloy, with lower fracture toughness values. These original experiments[1,2] were carried out in order to demonstrate the role of the T_o' curve in greatly influencing the mechanical properties of carbide-free bainitic steels. The experimental alloys developed for this purpose are not necessarily the optimum alloys from the point of industrial processing since they were obtained by isothermal heat treatments. The aim of this work is the design, using phase transformation theory, of a series of carbide free bainitic steels, given a set of industrial

constraints. The *incomplete reaction phenomenon* or T_o' concept[6-9)] has been used to optimise the microstructure by increasing the amount of bainitic ferrite in order to minimise the presence of blocks of austenite.

2. Thermodynamic and Kinetic Models on Phase Transformation in Steels

The mechanism by which bainite grows, places strict limits on the temperature range for transformation and on the maximum fraction of transformation that can ever be achieved. These criteria for bainite formation are embedded in the concept of T_o' curve. Thus, thermodynamic theory relying on the T_o' concept can be used to design an optimum microstructure, avoiding large regions of austenite known to be detrimental for toughness. At the same time, detailed kinetic theory must be used to ensure that the hardenability of the steel is sufficient for the specified industrial application and that the microstructure can be generated by continuous cooling transformation. In this sense, the reliability of different thermodynamic and kinetic models based on phase transformation have been reviewed and evaluated in this paper.

The Incomplete Reaction Phenomenon

The formation of bainite causes a deformation which is an IPS with a larger shear and a dilatational strain normal to the habit plane[6,10)]. This surface relief is considered an evidence of a martensitic mechanism of transformation. Bainite nucleation is considered to occur by the spontaneous dissociation of specific dislocation defects which are

already present in the parent phase. On the other hand, the subunit growth is considered diffusionless, although soon afterwards the excess of carbon is partitioned to the surrounded austenite, and stifled by the strength of the residual austenite[11,12]. Cementite can then precipitate from the enriched austenite between the ferrite plates. The process continues by successive nucleation of subunits until the carbon concentration of the residual austenite reaches the value at which the free energy of bainite becomes less than that of austenite of the same composition, i.e. the T_0 curve[7-9]. This trend is known as 'incomplete reaction phenomenon' because the transformation ends before the carbon concentration of austenite reaches the equilibrium value.

The T_o curve is the locus of points, on a temperature versus carbon concentration plot, where austenite and ferrite of the same chemical composition have the same free energy. The T_o' curve is defined similarly but taking into account the stored energy of the ferrite due to the displacive mechanism of transformation (400 J mol^{-1})[6]. It follows that the maximum amount of bainite that can be obtained at any temperature is limited by the fact that the carbon content of the residual austenite must not exceed the concentration given by the T_o' curve.

The T_o' concept can be used to minimise the amount of blocky, unstable austenite. An increase in the amount of bainitic ferrite is needed in order to consume the blocks of austenite.

Assuming that no other reaction interacts with the bainitic ferrite formation, the variation of the carbon content of austenite, $x_{\gamma,}$ as a function of the average carbon content of the alloy, $\bar{x}$, and the volume fraction of bainitic ferrite, $V_{b,}$ is given by:

$$x_\gamma = \bar{x} + V_b \frac{(\bar{x} - s)}{(1 - V_b)} \quad (1)$$

where s is the amount of carbon in solid solution in the bainitic ferrite (s ~ 0.03 wt-%)[1,2].

Equation (1) suggests two main methods of increasing the maximum permitted amount of transformation to bainitic ferrite: i) by reducing the overall carbon content $\bar{x}$ of the alloy concerned, so that the critical carbon concentration for displacive transformation is reached at a later stage (and hence a higher V_b). Of course, this is only useful if the reduction of the overall carbon content of the alloy does not lead to an unacceptable decrease in the strength of the steel; or ii) by modifying the substitutional alloying elements such that the T_o' curve is shifted to higher carbon concentrations in austenite.

The value of carbon concentration of the austenite, x_{T_0}, corresponding to the T_o temperature, is calculated from the following equation:

$$\Delta G^{\gamma \rightarrow \alpha} = 0 \quad (2)$$

where $\Delta G^{\gamma \rightarrow \alpha}$ is the free energy change accompanying the (austenite) $\gamma \rightarrow$ (ferrite) α transformation in which there is no change in the chemical composition and is calculated as a function of thermodynamic parameters such as the carbon-carbon interaction energy in austenite and ferrite, the free energy change accompanying the $\gamma \rightarrow \alpha$ transformation in pure iron and the partial molar enthalpy and entropy of solution of carbon in ferrite and austenite[10,13].

Time-Temperature-Transformation Diagrams

Apart from controlling the T_o' curve, substitutional solutes also affect hardenability, which is an important design parameter.

The thermodynamic model of solid-solid phase transformations in steels developed by Bhadeshia[13,14)] predicts the time-temperature-transformation diagram (TTT) from the knowledge of the chemical composition of the steel.

The times corresponding to the noses of the diffusional and diffusionless curves in the TTT diagrams are calculated as follows[14)],

$$t_{displ-TTT} = \exp\left[(243200/RT) - 135 + 20\log(T) - 5\log\left|\Delta G_m\right|\right] \quad (3)$$

$$t_{dif-TTT} = \exp\left[(603100/RT) - 190.5 + 20\log(T) - 4\log\left|\Delta G_m\right|\right] \quad (4)$$

where $t_{displ\text{-}TTT}$, in seconds, represents time for displacive transformations (Widmanstätten ferrite and bainite), $t_{dif\text{-}TTT}$, time for reconstructive transformations (allotriomorphic ferrite and pearlite), and ΔG_m is the available driving force for nucleation calculated as a function of the activity of carbon in ferrite and austenite.

The nucleation rate of both Widmanstätten ferrite and bainite becomes appreciable when:

$$\Delta G_m \leq G_N \quad (5)$$

where ΔG_m is the driving force for nucleation and G_N is the universal nucleation function[15].

A nucleus can develop into Widmanstätten ferrite if the driving force for paraequilibrium growth, $\Delta G^{\gamma \rightarrow \alpha + \gamma'}$, exceeds the stored energy of Widmanstätten ferrite, which has been estimated to be 50 J mol^{-1}.[6] The start temperature is identified as W_s. If the driving force for diffusionless growth, $\Delta G^{\alpha \rightarrow \gamma}$, exceeds the 400 J mol^{-1} of stored energy of bainite, then the transformation to bainite takes place and the start temperature is identified as bainite start temperature, B_s. The determination of martensite-start temperature, M_s, is similar to that used in the calculation of B_s, but in M_s determination the stored energy of martensite, G_{SM}, depends on the chemical composition of the steel.

Continuous Cooling Simultaneous Transformation Model

There are two applications of the Avrami extended space idea for grain boundary nucleated reactions, the first applying to the gradual elimination of free grain boundary area and the second to the gradual elimination of volume of untransformed material[16]. Using those ideas as a starting point, Jones and Bhadeshia[17] and Parker[18] developed a simultaneous transformation model which allows the prediction of the final microstructure and the ferrite grain size of the steel from the inputs of steel composition, prior austenite grain size and cooling schedule. The effect of eleven alloying elements is included in the model for the purposes of calculating the austenite/ferrite

paraequilibrium phase diagram, the associated free energy changes for both paraequilibrium and diffusionless transformations and the effect of substitutional solutes on the diffusivity of carbon in austenite. The austenite grains are assumed to be equiaxed and of uniform size, defined by the mean lineal intercept grain size, d_γ Proeutectoid ferrite, pearlite and bainite are modelled with a heterogeneous simultaneous kinetics approach, whereas the martensite transformation is calculated simply as a function of the undercooling below M_s. The necessary thermodynamic and kinetic parameters are calculated at fixed temperature steps below the paraequilibrium $Ae_3^{'}$ temperature until transformation is completed or stopped.

This model has been validated by Caballero *et al*.[19] in high strength low alloy (HSLA) steels, by comparison between experimental results and predictions given by the model. The model works extremely well when ferrite and pearlite are the final microstructures, but calculations incorrectly predict the formation of martensite instead of bainite. This problem is related to the fact that once M_s temperature is reached, all the remaining austenite transforms to martensite, even before bainite transformation is completed. Since the bainite transformation kinetics is controlled by nucleation rather than growth, it is believed that this problem must be related with an underestimation of the nucleation rate of bainite in the calculations. The bainite model only takes into account sheaves nucleated at the austenite grain boundary setting the autocatalysis factor to zero. Besides this limitation, the simultaneous transformation model has been used to select an optimum processing route for the designed steels since, at present, this model is one of the most complete continuous cooling transformation models.

3. Design of New Bainitic Steels

Recently, it has been demonstrated experimentally that models based on phase transformation theory can be successfully applied to the design of carbide free bainitic steels[20,21]. In this previous work, two steels alloyed with Ni were designed to achieve the highest combination of strength and toughness for bainitic microstructures. Toughness values of nearly 130 MPa $m^{1/2}$ were obtained for strength in the range of 1600-1700 MPa. Chemical composition and manufacturing conditions of the designed bainitic steels were selected to reach the same microstructure. Thus, the new alloys were designed to have the same bainitic transformation region in the *TTT* diagram and the same T_o' curve than those of Ni2 bainitic steel designed in previous work[20,21] and taken here as reference (Table 1). This steel proved to have impressive mechanical properties[20,21] when fully transforms to bainite.

For this purpose, we used the above described thermodynamic models that predict the *TTT* diagram and the T_o' curve from the chemical composition of the steel[13,14]. The output parameters of the models are: t_{dif}, which represents the minimum time at the ferrite and pearlite nose in the *TTT* diagram (Eq. (4)); t_{displ}, which represents the minimum time at the bainitic nose in the *TTT* diagram (Eq. (3)); and V_b, which indicates the maximum volume fraction of bainite formed at a given transformation temperature according to the T_o' curve (Eq. (1)). There are other out parameters such as the martensite and bainite start temperatures.

To ensure that the new alloys present the same bainitic transformation region in the *TTT* diagram and the same T_o' curve than those of the reference Ni2 steel, the chemical composition of the new alloys were selected to have t_{displ} and V_b parameters similar to those of Ni2 steel designed in previous work[20,21] and taken here as reference (Table 1).

Both parameters define bainite transformation according to thermodynamics. Moreover, the t_{dif} values of the new alloys must be high enough to avoid the formation of proeutectoid ferrite during cooling. Finally, the use of Ni as an alloying element has been avoided or reduced as much as possible for economical reasons.

Table 1 shows the chemical composition of the new designed steels. The C, Si and Mo contents of all the alloys were fixed to those in the Ni2 reference steel. A silicon content of 1.5 wt.% is the minimum content required to suppress carbide precipitation. Mo addition is made to reduce phosphorus embrittlement and to increase hardenability. Since this addition shifts the T_o' curve to lower austenite carbon concentrations, the Mo content was limited to 0.25 wt-%.

Steel CENIM 1 is a simple alloy with similar t_{displ} and V_{b400} parameters to those in Ni2 steel. Comparison of chemical composition in steels CENIM 2 and CENIM 3 suggests that the lower the Mn content, the higher the Cr content is needed in the alloy to get the same t_{displ} and V_{b400} parameters. In spite of its high cost, Ni is an alloying element used to increase the toughness and tensile strength without detrimental effect on the ductility. In this sense, 1.5 wt% Ni was added to the steel CENIM 3 and its Cr content was reduced in order to get the same t_{displ} and V_{b400} as those of Ni2 steel. This new steel was named CENIM 4.

Recent studies[22] on high carbon high silicon bainitic steels have shown that the addition of Co and Al increases the maximum volume fraction of bainitic ferrite and reduces the thickness of ferrite plates. With the aim of studying the influence of Co and Al, steels CENIM 5, CENIM 6 and CENIM 7 were designed with the same t_{displ} and V_{b400} parameters as those of the other alloys. Figure 1 shows *TTT* diagrams and the T_o' curves of the designed steels in comparison with those for Ni2 steel. The T_o' curve of the

different steels matches perfectly (Fig. 1(b)). Moreover, *TTT* diagrams in Fig. 1(a) show that all the new alloys have similar diffusionless curves and B_s and M_s temperatures, but different diffusional noses. This is not surprising since those steels have been designed to have the same maximum volume fraction of bainite at a given temperature.

On the other hand, *TTT* diagrams presented in Fig. 1(a) suggest that a two-steps cooling is the most promising processing route to obtain a full bainitic microstructure in the new alloys. An initial rapid cooling should be performed to avoid the formation of proeutectoid ferrite during cooling. The cooling should be slow down before B_s temperature is reached, in order to cross the bainitic zone of the *TTT* diagram. Finally, kinetic models for bainite transformation described above were used to estimate the volume fraction of bainite formed by different cooling routes. The input values in these models are: the chemical composition (C, Si, Mn, Cr, Ni, V and Mo), the prior austenite grain size and the cooling route. The influence of Co and Al in the transformation is not included in the calculations. According to the model a full bainitic microstructure (volume fraction of bainite higher than 0.75) will be formed applying the following cooling schedule during manufacturing procedure: first cooling rate: 30ºC/s; interrupted temperature: 600ºC; second cooling rate: 0.5ºC/s

4. Elaboration and Characterisation of the Designed Steels

Proposed alloys were manufactured by ARCELOR RESEARCH (France) as 180 x 80 x 12 mm^3 plates. The actual composition of the designed steels is shown in Table 2. All laboratory heats were elaborated in a 60 kg vacuum induction furnace under inert atmosphere (Ar, N_2). The generator power is 80 kW. Pure (>99.9 %) electrolytic iron

and addition of the alloying elements one after each other were used. Carbon deoxidation was performed and an analysis of C, S, N, O was made on line during elaboration for the final adjustment of composition. During elaboration, the temperature is controlled by a thermocouple.

Hot rolling simulations were firstly performed for CENIM 2, 5 and 7 on ARCELOR pilot plant according to the general scheme presented on Fig. 2. Apart from an air cooling, a coiling after accelerating cooling was tested on hot rolling simulation as processing route to obtain a fully bainitic microstructure in the new alloys. Specimens transverse to the hot rolling direction were ground and polished using standardised techniques for metallographic examination. A 2 percent Nital etching solution was used to reveal the microstructure by optical microscopy. Scanning electron microscopy observation was carried out on a Jeol JSM-6500F field emission scanning electron microscope operating at 7 kV.

Quantitative X-ray analysis was used to determine the fraction of retained austenite. For this purpose, 11 x 5 x 2 mm^3 samples were machined. After grinding and final polishing using 1 μm diamond paste, the samples were etched to obtain an undeformed surface. They were then step-scanned in a SIEMENS D 5000 X-ray diffractometer using unfiltered Cu K_α radiation. The scanning speed (2θ) was less than 0.3 degree/min. The machine was operated at 40 kV and 30 mA. The retained austenite content was calculated from the integrated intensities of (200), (220) and (311) austenite peaks, and those of (002), (112) and (022) planes of ferrite.

Specimens for transmission electron microscopy (TEM) were machined down to 3 mm diameter rod. The rods were sliced into 400 μm thick discs and subsequently ground down to foils of 50 μm thickness on wet 1200 grit silicon carbide paper. These foils

were finally electropolished at room temperature until perforation occurred, using a twin-jet electropolisher set at a voltage of 40 V. The electrolyte consisted of 5 % perchloric acid, 15 % glycerol and 80 % methanol. The foils were examined in a JEOL JEM 2010 transmission electron microscope at an operating voltage of 200 kV.

Experimental data for the first set of manufactured strips are presented in Table 3. As an example, Fig. 3 shows optical and scanning electron micrographs of the microstructure obtained after air cooling from 600 ºC in the first set of manufactured steels. Experimental results reveal that steels CENIM 2 and CENIM 5 after air cooling from every temperature tested have the desired microstructure consisting of mainly bainitic ferrite and retained austenite. Due to the high volume fraction of bainitic ferrite in those samples, more than 0.68, the film shaped retained austenite is expected to be present between the subunits of bainitic ferrite. By contrast, the small amount of bainite in the CENIM 7 steel after air-cooling from every temperature (Table 3) causes much of the blocky residual austenite to transform to martensite during cooling because of lower carbon-enrichment.

On the other hand, it seems that whatever the steel grades are, proeutectoid ferrite is formed during coiling at 550 ºC. This coiling temperature is probably too high and the cooling rate achieved is too slow to avoid diffusional transformations during coiling.

The expected typical mixtures of bainite, martensite and retained austenite have been obtained in all other cases. Since the CENIM 2, 5 and 7 steels were designed to have a similar bainitic nose in the *TTT* diagram (see Fig. 1(a)), it seems reasonable that these steels exhibit similar hardenability. However, the high alloying content slows down the kinetics of bainite formation in the CENIM 7. This would explain the higher volume fraction of martensite formed in this steel.

The CENIM 2 and CENIM 5 steels after air cooling are bainitic steels with a microstructure similar to that of the reference steel Ni2[20,21]. Nevertheless, the retained austenite fraction is low compared with the martensite fractions, specially at higher FCTs (see Table 3). The residual austenite after bainite formation is not sufficiently enriched with carbon and thus transforms into martensite during air cooling. In this sense, lower FCTs are recommended to increase the thermal stability of austenite.

Figure 4 shows transmission electron micrographs of the steels CENIM 2 and 5 after air cooling from different temperatures. Bright-field images confirm that the microstructure in both steels consists of carbide-free upper bainite with interlath retained austenite films (see for example Figs. 4(a) and 4(c)). These films have sometimes a typical wavy morphology characteristic of the bainite in high-silicon steels. Just a few sheaves of lower bainite with fine carbides precipitated inside ferritic plates (see Fig. 4(d)) and some blocky tempered martensite (see Fig. 4(b)) has been observed. Likewise, Fig. 5 shows bright-field images of the CENIM 7 steel after air cooling from different temperatures. Microstructures mainly consist of martensite and/or tempered martensite. An example of blocky tempered martensite is shown in Fig. 5(b), where the typical multi-variant carbide precipitation is observed. Moreover, sheaves of carbide-free upper bainite with interlath retained austenite films are present in the microstructure (see Fig. 5(a)). Finally, a few sheaves of lower bainite with fine carbides precipitated inside ferritic plates (see Fig. 5(c)) are observed.

Characterisation of New Set of Strips using Optimized Conditions

Based on experimental results described above, a new set of strips was manufactured. Again, hot rolling simulations have been performed according to the general scheme presented in Fig. 2. However, at this time the first cooling rate has been increased up to 70 ºC/s and in some cases, coiling temperature has been decreased to avoid ferrite formation. Likewise, the FCT has been decreased to get lower the martensite fraction. The thickness of the strips remains unchanged.

Experimental data on the microstructure are presented in Table 4. Figures 6 and 7 show optical and electron micrographs of fully carbide free bainitic microstructures (more than 75 % of bainitic ferrite) in the seven designed steels. Microstructural characterisation revealed that, as in the first set of strips, the CENIM 2 and 5 after air cooling from every temperature tested have the desired microstructure consisting of carbide free upper bainite. Due to the high volume fraction of bainitic ferrite in those samples, film shaped retained austenite is present between the subunits of bainitic ferrite free of carbides, as TEM micrographs confirm (Figs 6(f) and 7(f)). Again, the small amount of bainite in CENIM 7 after air-cooling have caused much of the blocky residual austenite to transform to martensite during cooling because of the low carbon-enrichment. By contrast, a higher volume fraction of bainite has been obtained by decreasing the coiling temperatures in the hot rolling simulation of this steel. In that case, a desired bainitic microstructure is obtained (Fig. 7(l)). Again, it has not been possible to totally avoid proeutectoid ferrite formation in CENIM 5 after coiling (see Table 4).

Quantitative metallographic results in Table 4 also reveal that the CENIM 1, 3, 4 and 6, after air cooling from every temperature tested have the desired microstructure consisting of mainly bainitic ferrite and retained austenite. The retained austenite is expected to be present as films between the subunits of bainitic ferrite because of the

high volume fraction of bainitic ferrite, higher than 0.80 in most of the cases. TEM micrographs confirm the absence of carbides in these bainitic microstructures (Figs. 6(c), 6(i) and 7(c)). Moreover, as expected, retained austenite is present as films between the subunits of bainitic ferrite. Finally, it is important to mention that it has not been possible to avoid proeutectoid ferrite formation in steels CENIM 1, 3 and 4 steels after coiling. It seems that the coiling temperature tested has not been low enough to avoid the presence of proeutectoid ferrite. However, it has been obtained the desired bainitic microstructure in the steel CENIM 6 after coiling (Fig. 7(i)).

Validity of the Design Procedure

As it was above mentioned, all the steels were designed to have identical time at the bainitic nose in the *TTT* diagram (t_{displ}) and identical maximum volume fraction of bainite formed at 400ºC (V_{b400}) parameters according to the T_o' curve as those in the reference steel (Ni2 steel). The C, Si and Mo contents of these alloys were fixed to those in the reference steel (Ni2 steel). Comparison of the chemical composition of steels CENIM 1, 2 and 3 suggests that the lower the Mn content, the higher the Cr content is needed in the steel to achieve the same t_{displ} and V_{b400} parameters. Likewise, comparison of the chemical composition of steels CENIM 2, 5 and 6 suggests the higher the Co content, the higher the Cr content is needed in the alloy to reach both thermodynamic parameters. Finally, it has been found that the addition of Ni requires a decrease in Cr content to keep the same bainitic region in the *TTT* diagram of CENIM 3 and 4. Fig. 8 shows the volume fraction of bainite formed during air-cooling in the designed steels and the hardness values of the resulting microstructure. Results suggested that similar

bainitic microstructures were obtained in six of the steels for all the tested routes. Differences in the microstructure are attributed to the slight differences in the actual chemical composition and the processing parameters of the experimental alloys. The designed steels are bainitic steels with a microstructure similar to that of the reference steel Ni2. These results confirm the success in the design procedure.

Mechanical Properties Characterisation

The mechanical properties of samples with a bainitic and martensitic microstructure have been characterised on normalized cylindrical TB5 tensile samples in accordance with the steel standard ASTM E8. The measured tensile properties are reported in Table 5 together with those for the reference material. The values presented are average for 3 tests. The tensile tests have been performed at room temperature and low strain rate ($0.008\ s^{-1}$).

Plates of bainitic ferrite are typically 10 μm in length and about 0.2 μm in thickness (see TEM micrographs). This gives a rather small mean free path for dislocation glide. Thus, the main microstructural contribution to the strength of bainite is from the extremely fine grain size of bainitic ferrite. It is difficult to separate the effect of retained austenite on strength in these steels from other factors. Qualitatively, austenite can affect the strength in several ways. Residual austenite can transform to martensite during cooling to room temperature, thus increasing the strength (see the result for the steel CENIM 7 after air cooling in Table 5). On the other hand, retained austenite interlath films can increase the strength by transforming to martensite during testing, similar to the behaviour of TRIP steels.

The low yield/ultimate tensile strength ratios (YS/UTS) in Table 5 are due to the presence of austenite and the generally large dislocation density in the microstructure. Consequently, retained austenite increases the strain-hardening rate of the steel. Likewise, tensile elongation is controlled by the volume fraction of retained austenite. Retained austenite is a ductile phase compared to the bainitic ferrite and would be expected to enhance ductility as far as the austenite is homogeneously distributed along plate boundaries (film austenite). However, isolated pools of austenite (blocky austenite) would influence unfavourably on both elongation and UTS. From Table 5, it is clear that the steels present a combination of high strength and good ductility.

Impact toughness was measured on normalized Charpy notched (10 x 10 mm^2) samples at temperatures between 20ºC and -120ºC using a 300 J Charpy testing machine. Specimens were tested in accordance with the steel standard BS EN 10 045-1: 1990. Six specimens were tested at each temperature for every alloy.

Charpy impact test results are also listed in Table 5 for all the alloys. A considerable improvement in toughness is obtained when the volume fraction of bainite is high. This improvement occurs despite the fact that the strength of the microstructures involved remains quite high. From the data in Table 5, it is evident that the volume fraction of bainite V_b and thus the carbon content of the retained austenite x_γ explain the improvement in toughness observed in alloys with a mainly bainitic microstructure (CENIM 1-6 after air cooling) as compared with those with a mainly martensitic microstructure (CENIM 7 after air cooling). The results are consistent with the enhancement of toughness expected when the amount of blocky austenite and martensite are reduced and, in general, when the thermal and mechanical stability of residual austenite is increased.

5. Conclusions

With this work, it has been demonstrated that models based on phase transformation theory can be applied successfully to the design of high strength-high toughness carbide free bainitic steels. Using these models, a set of seven carbide free bainitic steels with a 0.3 wt-% carbon content have been proposed for manufacturing. Except for the steel with the highest content of alloying elements (the steel CENIM 7), all the grades present the same microstructure composed of carbide-free upper bainite and retained austenite after hot rolling and a two-steps cooling. The designed steels present significant combinations of strength and ductility. The tensile strengths ranging from 1600 MPa to 1950 MPa are obtained while keeping a total elongation over 10 %. Impact toughness properties at room temperature of newly designed steels are comparable to those of quenched and tempered martensitic steels.

Acknowledgements

The authors gratefully acknowledge the support of the Research Fund for Coal and Steel for funding this research under the contract 7210-PR/345. M.J. Santofimia would also like to express her gratitude to Consejo Superior de Investigaciones Científicas (CSIC) for the financial support in the form of a PhD Research Grant (I3P Program). C. Garcia-Mateo would like to thank Spanish Ministerio de Ciencia y Tecnología for the financial support in the form of a Ramón y Cajal contract (RyC 2004 Program).All of us want to

thank to T. Iung and S. Allain (ARCELOR RESEARCH) for manufacturing the designed alloys and their help on mechanical testing.

References

(1) H. K. D. H. Bhadeshia and D. V. Edmonds: *Met. Sci*., **17**(1983), 411.

(2) H. K. D. H. Bhadeshia and D. V. Edmonds: *Met. Sci*., **17**(1983), 420.

(3) V. T. T. Miihkinen and D. V. Edmonds: *Mater. Sci. Technol*., **3**(1987), 422.

(4) V. T. T. Miihkinen and D. V. Edmonds, *Mater. Sci. Technol*., **3**(1987), 432.

(5) V. T. T. Miihkinen and D. V. Edmonds, *Mater. Sci. Technol*., **3**(1987), 441.

(6) H. K. D. H. Bhadeshia: *Acta Metall*., **29**(1981), 1117.

(7) H. K. D. H. Bhadeshia and A. R. Waugh: *Acta Metall*., **30**(1982), 775.

(8) L. C. Chang and H. K. D. H. Bhadeshia: *Mater. Sci. Eng. A*, **184**(1994), L17.

(9) I. Stark, G. D. W. Smith and H. K. D. H. Bhadeshia: Proc. of Int. Conf. Phase Transformation, Ed. by G. W. Lorimer, Institute of Metals, London (1988), 211.

(10) H. K. D. H. Bhadeshia and D. V. Edmonds: *Acta Metall*., **28**(1980), 1265.

(11) H. K. D. H. Bhadeshia and J. W. Christian: *Metall. Trans. A*, **21**(1990) 767-97.

(12) S. B. Singh, H. K. D. H. Bhadeshia: *Mater. Sci. Eng. A*, **12**(1996) 610-612.

(13) Materials Algorithms Project (MAP), Department of Materials Science and Metallurgy, University of Cambridge, U. K.: http://www.msm.cam.ac.uk/map.

(14) H. K. D. H. Bhadeshia: *Met. Sci.*, **16**(1982), 159.

(15) A. Ali and H. K. D. H. Bhadeshia: *Mat. Sci. Technol*., **6**(1990), 781.

(16) J. W. Cahn: *Acta Metall.*, **4(**1956), 449.

(17) S. J. Jones and H. K. D. H. Bhadeshia: *Acta Metall*., **45**(1997), 2911.

(18) S. V. Parker: ‘Modelling of Phase Transformation in Hot Rolled Steels’, PhD Thesis, University of Cambridge, U. K., (1997).

(19) F. G. Caballero, C. Capdevila and C. García de Andrés: *Mat. Sci. Technol*., **18**(2002), 534.

(20) F. G. Caballero, H. K. D. H. Bhadeshia, K. J. A. Mawella, D. G. Jones and P. Brown: *Mat. Sci. Technol*., **17**(2001) 512.

(21) F. G. Caballero, H. K. D. H. Bhadeshia, K. J. A. Mawella, D. G. Jones and P. Brown: *Mat. Sci. and Technol*., **17**(2001), 517.

(22) C. García-Mateo, F. G. Caballero and H. K. D. H. Bhadeshia: *ISIJ Int*., **43**(2003), 1821.

Table 1. Chemical composition of designed alloys and reference material, (mass-%).

Table 2. Chemical composition, (mass-%).

Table 3. Quantitative data on microstructure and hardness.

Table 4. Quantitative data on microstructure and hardness.

Table 5. Tensile properties and Charpy impact test results.

Fig. 1. (a) *TTT* diagram and (b) T_o' curve of the designed steels.

Fig. 2. General scheme of the hot rolling simulation. FRT stands for finishing rolling temperature; and FCT stands for finishing cooling temperature.

Fig. 3. Optical and electron micrographs of the first set of manufactures steels after air cooling from 600 ºC: (a, b) CENIM 2, (c, d), CENIM 5, and (e, f), CENIM 7.

Fig. 4. Transmission electron micrographs of CENIM 2 and CENIM 5 after air cooling from different temperatures.

Fig. 5. Transmission electron micrographs of CENIM 7 after air cooling from: (a) 550 ºC; (b) 600 ºC; and (c) 650 ºC.

Fig. 6. Optical and electron micrographs of the designed steels after air cooling from different temperatures: (a-c) CENIM 1 / AC 600 ºC, (d-f) CENIM 2 / AC 550 ºC, (g-i) CENIM 3 / 500 ºC.

Fig. 7. Optical and electron micrographs of the designed steels after air cooling: (a-c) CENIM 4 / AC 500 ºC, (d-f) CENIM 5 / AC 500 ºC; and after coiling: (g-i) CENIM 6 / CT 500 ºC, and (j-l) CENIM 7 /CT 350 ºC.

Fig. 8. (a) Volume fraction of bainite and (b) Vickers hardness of microstructures formed by air-cooling in the designed steels.

Tables

Table 1. Chemical composition of designed alloys and reference material, (mass-%).

Steel	C	Si	Mn	Ni	Cr	Mo	Co	Al
Ni2 (Reference)	0.30	1.50	---	3.50	1.44	0.25	---	---
CENIM 1	0.30	1.50	2.23	---	---	0.25	---	---
CENIM 2	0.30	1.50	2.00	---	0.46	0.25	---	---
CENIM 3	0.30	1.50	1.50	---	1.46	0.25	---	---
CENIM 4	0.30	1.50	1.50	1.50	0.17	0.25	---	---
CENIM 5	0.30	1.50	2.00	---	1.16	0.25	1.00	---
CENIM 6	0.30	1.50	2.00	---	1.51	0.25	1.50	---
CENIM 7	0.30	1.50	2.00	1.76	1.51	0.25	1.50	1.00

Table 2. Chemical composition, (mass-%).

Steel	C	Si	Mn	Ni	Cr	Mo	Co	Al
CENIM 1	0.290	1.5	2.25	---	---	0.26	---	---
CENIM 2	0.29	1.46	1.97	---	0.46	0.25	---	---
CENIM 3	0.290	1.49	1.56	---	1.47	0.25	---	---
CENIM 4	0.27	1.71	1.53	1.47	0.17	0.245	---	---
CENIM 5	0.29	1.47	1.97	---	1.20	0.25	0.97	---
CENIM 6	0.285	1.50	2.04	---	1.50	0.245	1.48	---
CENIM 7	0.30	1.44	2.06	1.7	1.6	0.24	1.43	1.01

Table 3. Quantitative data on microstructure and hardness of first strips.

Steel / Cooling - FCT	V_F	V_B	V_M	V_γ	x_γ, wt-%	Hardness, HV30
Ni2 (Reference)	---	0.81 ± 0.06	0.08 ± 0.05	0.11 ± 0.01	1.03 ± 0.03	536 ± 6
CENIM 2 (1st Strip) / CT 550 ºC	0.54 ± 0.07	0.13 ± 0.04	0.33 ± 0.04	NM	NM	388 ± 4
CENIM 2 (1st Strip) / AC 550 ºC	---	0.88 ± 0.05	0.07 ± 0.04	0.05 ± 0.01	0.97 ± 0.03	521 ± 9
CENIM 2 (1st Strip) / AC 600 ºC	---	0.86 ± 0.03	0.08 ± 0.02	0.07 ± 0.01	0.95 ± 0.01	478 ± 17
CENIM 2 (1st Strip) / AC 650 ºC	---	0.80 ± 0.08	0.15 ± 0.07	0.05 ± 0.01	0.82 ± 0.03	550 ± 12
CENIM 5 (1st Strip) / CT 550 ºC	0.47 ± 0.05	0.20 ± 0.05	0.35 ± 0.05	NM	NM	413 ± 2
CENIM 5 (1st Strip) / AC 550 ºC	---	0.74 ± 0.05	0.18 ± 0.04	0.07 ± 0.01	1.05 ± 0.03	522 ± 14
CENIM 5 (1st Strip) / AC 600 ºC	---	0.80 ± 0.05	0.20 ± 0.05	0.05 ± 0.01	1.05 ± 0.03	527 ± 9
CENIM 5 (1st Strip) / AC 650 ºC	---	0.68 ± 0.05	0.25 ± 0.05	0.07 ± 0.01	1.02 ± 0.03	525 ± 11
CENIM 7 (1st Strip) / CT 550 ºC	0.45 ± 0.09	0.19± 0.10	0.36 ± 0.04	NM	NM	432 ± 1
CENIM 7 (1st Strip) / AC 550 ºC	---	0.38 ± 0.07	0.55 ± 0.06	0.07 ± 0.01	0.96 ± 0.03	556 ± 6
CENIM 7 (1st Strip) / AC 600 ºC	---	0.42 ± 0.06	0.51 ± 0.05	0.07 ± 0.01	0.93 ± 0.03	552 ± 4
CENIM 7 (1st Strip) / AC 650 ºC	---	0.41 ± 0.07	0.52 ± 0.06	0.07 ± 0.01	0.96 ± 0.03	554 ± 4

FCT stands for finishing cooling temperature; CT stands for coiling temperature; AC stands for air cooling; V_F is the volume fraction of proeutectoid ferrite; V_B is the volume fraction of bainitic ferrite; V_M is the volume fraction of martensite; V_γ is the volume fraction of austenite; x_γ is the carbon content in austenite; and NM stands for 'no measurements'.

Table 4. Quantitative data on microstructure and hardness of new strips.

Steel / Cooling - FCT	V_F	V_B	V_M	V_γ	x_γ, wt-%	Hardness, HV30
Ni2 (Reference)	---	0.81 ± 0.06	0.08 ± 0.05	0.11 ± 0.01	1.03 ± 0.03	536 ± 6
CENIM 1 / CT 550 ºC	0.59 ± 0.03	0.04 ± 0.01	0.36± 0.03	NM	NM	379 ± 8
CENIM 1 / AC 450 ºC	---	0.73 ± 0.04	0.24 ± 0.05	0.03 ± 0.01	0.66 ± 0.06	530 ± 7
CENIM 1 / AC 600 ºC	---	0.76 ± 0.03	0.21 ± 0.04	0.03 ± 0.01	0.95 ± 0.01	522 ± 4
CENIM 2 (2^{nd} Strip) / AC 500 ºC	---	0.77± 0.04	0.13 ± 0.05	0.10 ± 0.01	1.14 ± 0.03	519 ± 3
CENIM 2 (2^{nd} Strip) / AC 550 ºC	---	0.80 ± 0.04	0.09 ± 0.05	0.10 ± 0.01	1.26 ± 0.07	460 ± 20
CENIM 3 / CT 500 ºC	0.50 ± 0.04	0.08 ± 0.02	0.43 ± 0.03	NM	NM	416 ± 4
CENIM 3 / AC 500 ºC	---	0.88 ± 0.02	0.02 ± 0.03	0.11 ± 0.01	1.03 ± 0.05	495 ± 15
CENIM 3 / AC 550 ºC	---	0.86± 0.02	0.03 ± 0.04	0.11 ± 0.01	1.04 ± 0.04	505 ± 6
CENIM 4 / CT 550 ºC	0.34 ± 0.03	0.12 ± 0.02	0.54 ± 0.04	NM	NM	391 ± 2
CENIM 4 / AC 500 ºC	---	0.88 ± 0.02	0.09 ± 0.04	0.03 ± 0.003	1.26 ± 0.07	531 ± 10
CENIM 5 (2^{nd} Strip) / CT 550 ºC	0.45 ± 0.05	0.10 ± 0.03	0.45 ± 0.06	NM	NM	437 ± 3
CENIM 5 (2^{nd} Strip) / AC 500 ºC	---	0.81± 0.05	0.10 ± 0.06	0.08 ± 0.01	1.18 ± 0.07	521 ± 12
CENIM 5(2^{nd} Strip) / AC 550 ºC	---	0.76 ± 0.05	0.20 ± 0.06	0.04 ± 0.01	0.80 ± 0.06	555 ± 11
CENIM 6/ CT 500ºC	---	0.88 ± 0.01	Traces	0.09 ± 0.01	1.0 ± 0.3	503 ± 4
CENIM 6 / AC 500 ºC	---	0.86 ± 0.02	0.07 ± 0.04	0.08 ± 0.01	1.6 ± 0.3	555 ± 14
CENIM 7(2^{nd} Strip) / CT 350 ºC	---	0.77 ± 0.04	---	0.27 ±0.02	1.11 ± 0.03	412 ± 5
CENIM 7 (2^{nd} Strip) / AC 500 ºC	---	0.62 ± 0.04	0.30 ±0.04	0.09 ±0.01	0.98 ±0.07	559 ± 8
CENIM 7 (2^{nd} Strip) / AC 600 ºC	---	0.56 ±0.05	0.39 ±0.06	0.05 ±0.01	0.75 ±0.11	563 ± 7

FCT stands for finishing cooling temperature; CT stands for coiling temperature; AC stands for air cooling; V_F is the volume fraction of proeutectoid ferrite; V_B is the volume fraction of bainitic ferrite; V_M is the volume fraction of martensite; V_γ is the volume fraction of austenite; x_γ is the carbon content in austenite; and NM stands for 'no measurements'.

Table 5. Tensile properties and Charpy impact test results.

Steel / Cooling - FCT	YS, MPa	UTS, MPa	YS/UTS	Total Elongation, %	Impact Energy, J					
					-20ºC	0ºC	20ºC	50ºC	100ºC	150ºC
Ni2 (Referente)	1028	1476	0.70	17.8	---	---	50	---	---	---
CENIM 1 / AC 450 ºC	1084	1808	0.60	11	---	29	36	---	42	38
CENIM 1 / AC 600 ºC	1021	1696	0.60	11	---	16	22	---	41	48
CENIM 2 (2^{nd} Strip) / AC 500 ºC	1020	1627	0.63	11.6	---	---	36	39	55	55
CENIM 2 (2^{nd} Strip) / AC 550 ºC	1132	1613	0.70	10.3	---	30	44	47	53	43
CENIM 3 / AC 500 ºC	1068	1671	0.64	12.2	32	39	44	---	61	61
CENIM 3 / AC 550 ºC	1077	1698	0.63	10.8	---	33	46	---	65	64
CENIM 4 / AC 500ºC	1097	1710	0.64	13.9	---	---	38	---	---	---
CENIM 5 (2^{nd} Strip) / AC 500 ºC	1059	1696	0.62	11.6	---	---	40	40	65	56
CENIM 5(2^{nd} Strip) / AC 550 ºC	1105	1801	0.61	11	---	---	31	---	36	38
CENIM 6/ CT 500ºC	834	1495	0.56	13.6	---	---	24	---	---	---
CENIM 6 / AC 500 ºC	1074	1799	0.60	10.7	---	---	25	---	---	---
CENIM 7(2^{nd} Strip) / CT 350 ºC	851	1531	0.56	13.6	---	---	31	---	51	58
CENIM 7 (2^{nd} Strip) / AC 500 ºC	1125	1929	0.58	9.7	---	---	25	---	30	30
CENIM 7 (2^{nd} Strip) / AC 600 ºC	1203	1945	0.62	7	---	---	26	---	24	28

FCT stands for finishing cooling temperature; CT stands for coiling temperature; AC stands for air cooling; YS yield strength; UTS ultimate tensile strength;

Figures

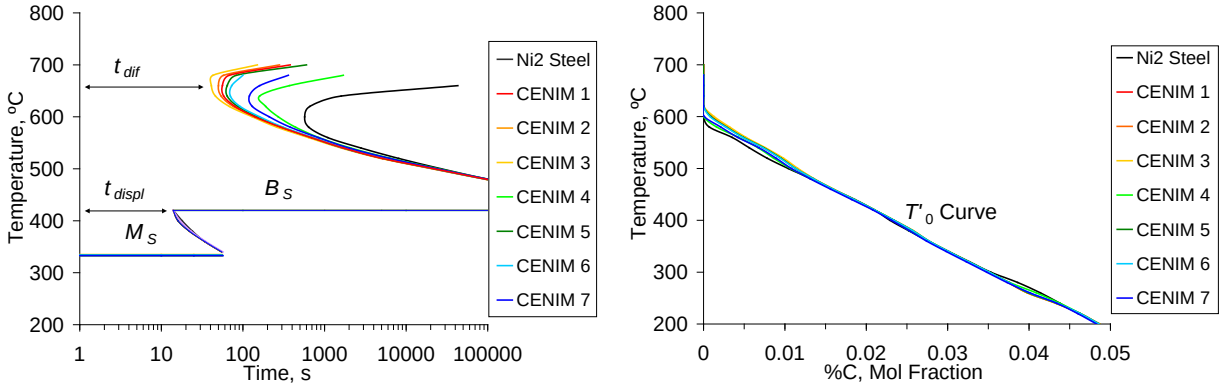

(a) (b)

Fig. 1. (a) *TTT* diagram and (b) T_o' curve of the designed steels.

Caballero *et al*.

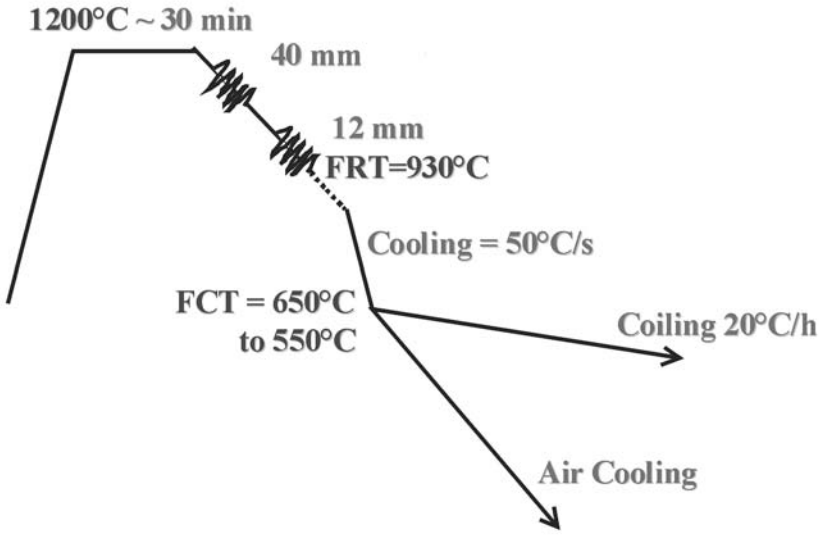

Fig. 2. General scheme of the hot rolling simulation. FRT stands for finishing rolling temperature; and FCT stands for finishing cooling temperature.

Caballero *et al*.

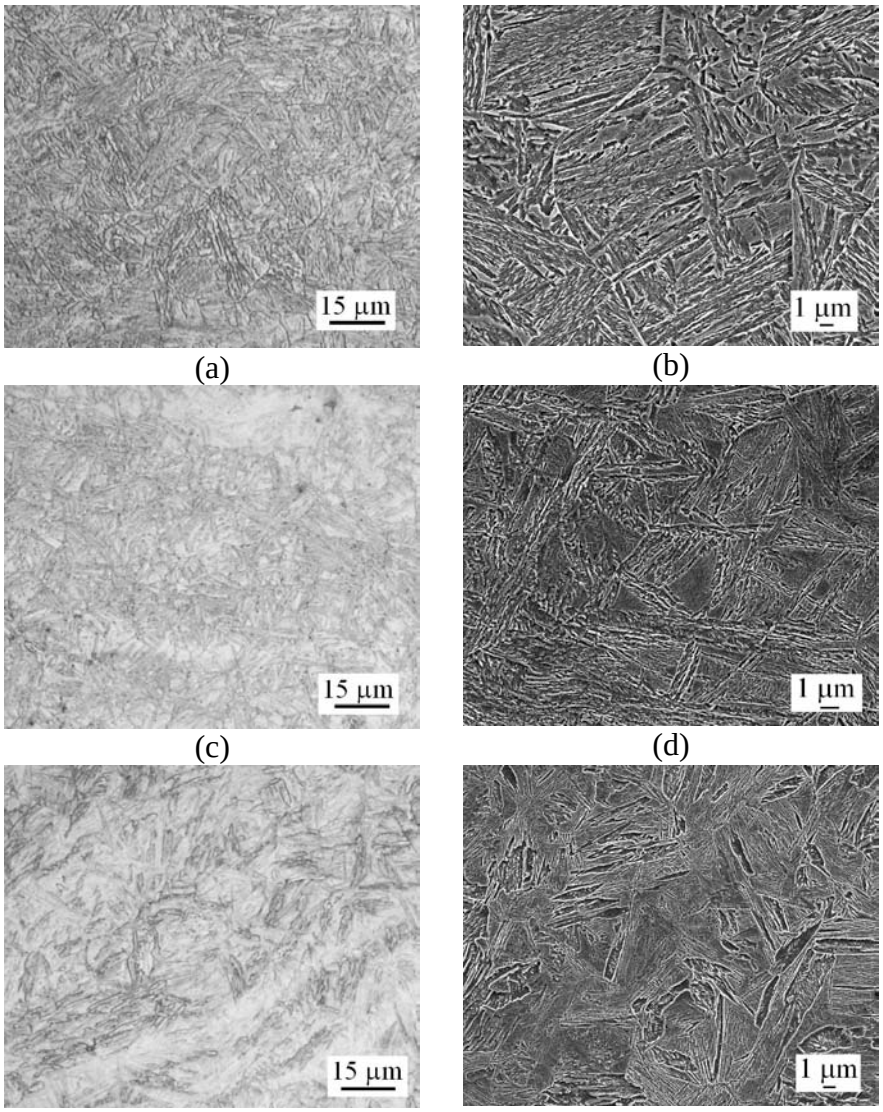

Fig. 3. Optical and electron micrographs of the first set of manufactures steels after air cooling from 600 ºC: (a, b) CENIM 2, (c, d) CENIM 5, and (e, f) CENIM 7. First strips.

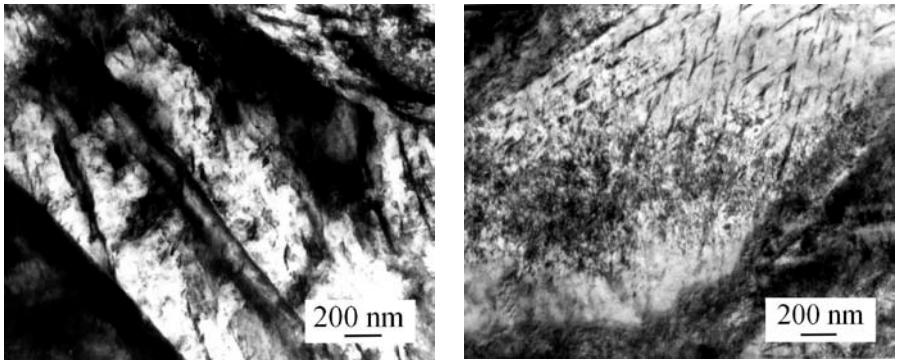

(a) CENIM 2 / AC 550 ºC (b) CENIM 2 / AC 650 ºC

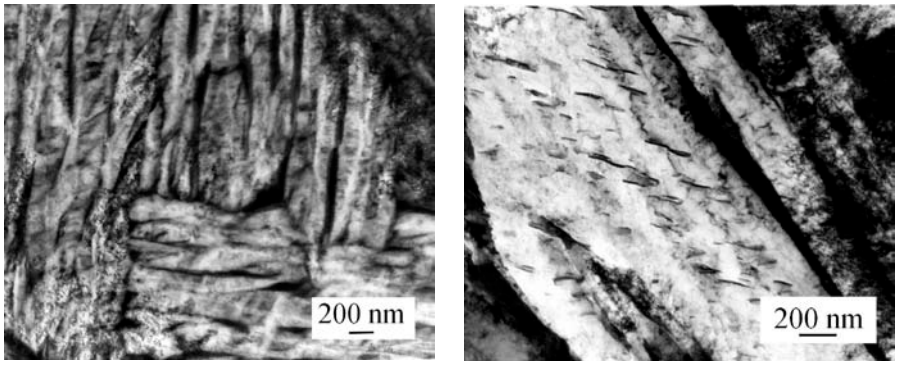

(c) CENIM 5 / AC 550 ºC (d) CENIM 5 / AC 600 ºC

Fig. 4. Transmission electron micrographs of CENIM 2 and CENIM 5 after air cooling from different temperatures. First strips.

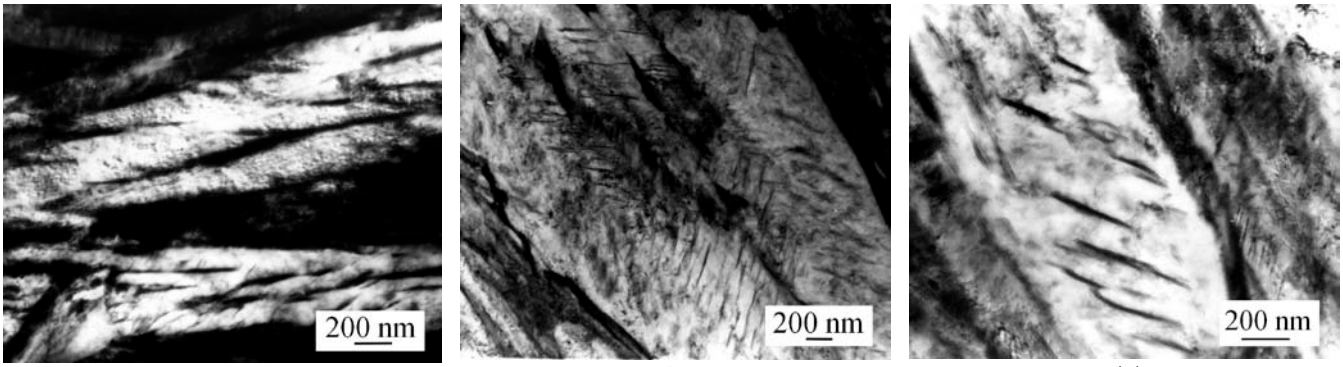

(a) (b) (c)

Fig. 5. Transmission electron micrographs of CENIM 7 after air cooling from: (a) 550 ºC; (b) 600 ºC; and (c) 650 ºC. First strips.

Caballero *et al*.

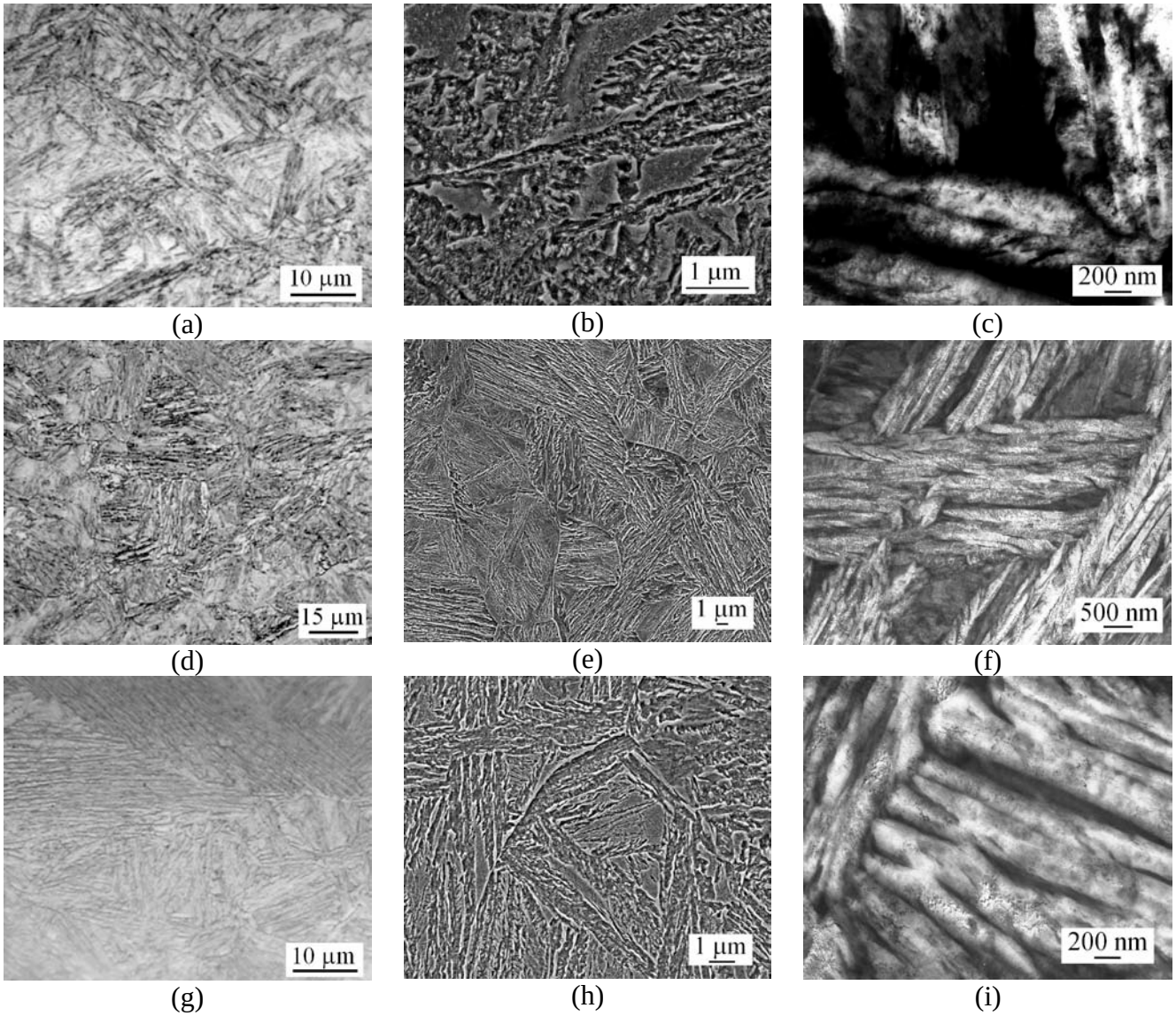

Fig. 6. Optical and electron micrographs of the designed steels after air cooling from different temperatures: (a-c) CENIM 1 / AC 600 ºC, (d-f) CENIM 2 / AC 550 ºC, (g-i) CENIM 3 / 500 ºC. New strips.

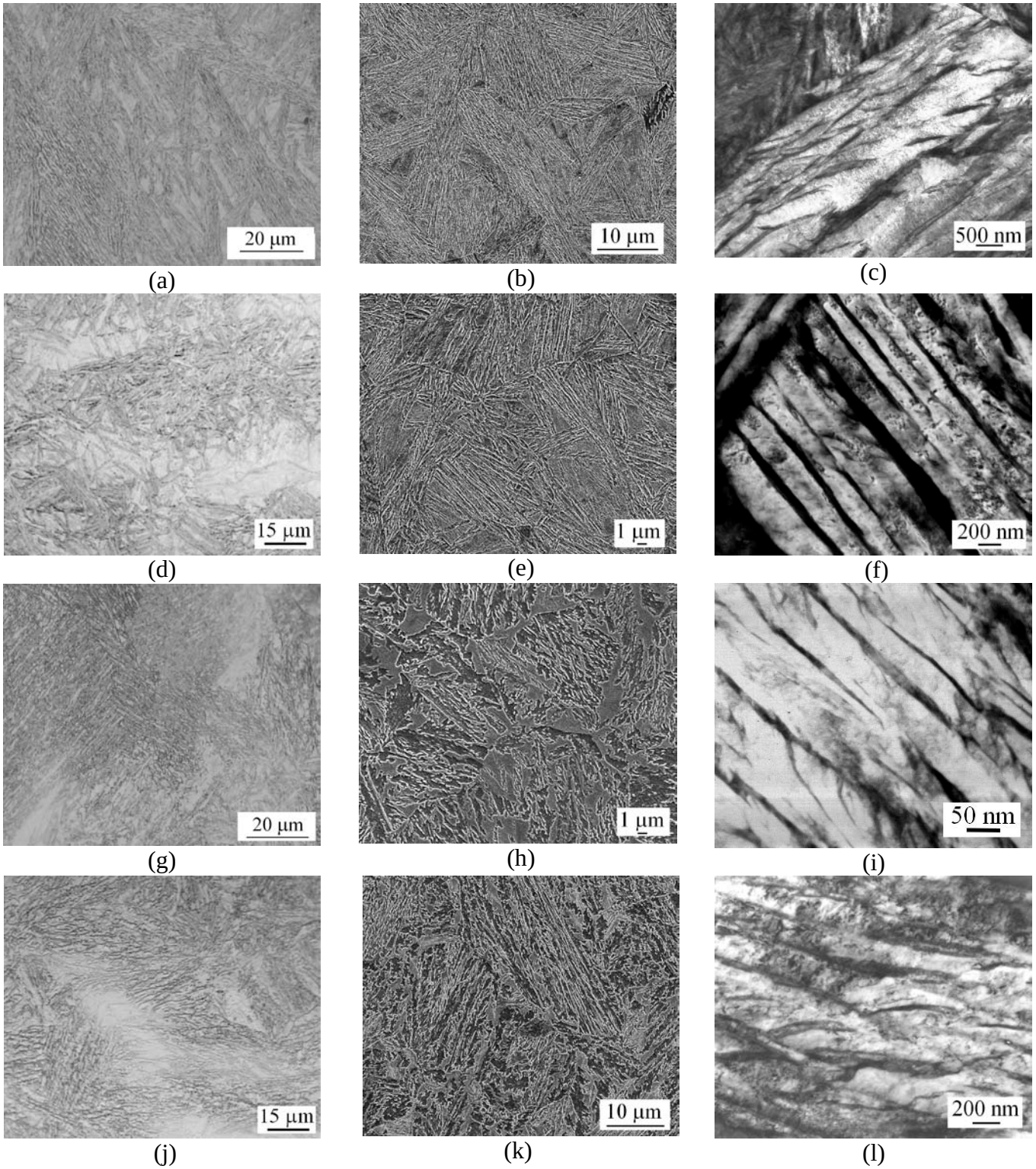

Fig. 7. Optical and electron micrographs of the designed steels after air cooling: (a-c) CENIM 4 / AC 500 ºC, (d-f) CENIM 5 / AC 500 ºC; and after coiling: (g-i) CENIM 6 / CT 500 ºC, and (j-l) CENIM 7 /CT 350 ºC. New strips.

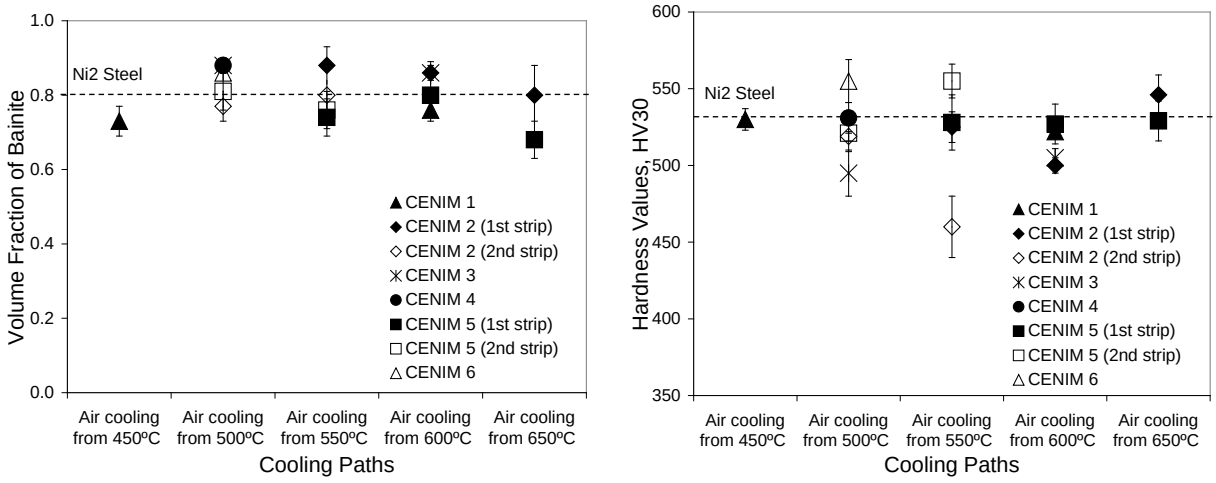

(a) (b)

Fig. 8. (a) Volume fraction of bainite and (b) Vickers hardness of microstructures formed by air-cooling in the designed steels.